J. Fluid Mech. (1974), *vol.* 63, *part* 4, *pp.* 801–825
Printed in Great Britain

Nonlinear interactions among standing surface and internal gravity waves†

By TERRENCE M. JOYCE

Department of Meteorology, Massachusetts Institute of Technology‡

(Received 7 September 1973)

A laboratory study has been undertaken to measure the energy transfer from two surface waves to one internal gravity wave in a nonlinear, resonant interaction. The interacting waves form triads for which

$$\sigma_{1s} - \sigma_{2s} \pm \sigma_I = 0 \quad \text{and} \quad \kappa_{1s} - \kappa_{2s} \pm \kappa_I = 0;$$

σ_j and κ_j being the frequency and wavenumber of the jth wave. Unlike previously published results involving single triplets of interacting waves, all waves here considered are *standing* waves. For both a diffuse, two-layer density field and a linearly increasing density with depth, the growth to steady state of a resonant internal wave is observed while two deep water surface eigenmodes are simultaneously forced by a paddle. Internal-wave amplitudes, phases and initial growth rates are compared with theoretical results derived assuming an arbitrary Boussinesq stratification, viscous dissipation and slight detuning of the internal wave. Inclusion of viscous dissipation and slight detuning permit predictions of steady-state amplitudes and phases as well as initial growth rates. Satisfactory agreement is found between predicted and measured amplitudes and phases. Results also suggest that the internal wave in a resonant triad can act as a catalyst, permitting appreciable energy transfer among surface waves.

1. Introduction

In the past twelve years, resonant wave–wave interactions in fluid mechanics have been studied a great deal. The original suggestion by Phillips (1960) that irrotational surface gravity waves would exhibit such an interaction was the first in a series of papers on resonantly interacting surface gravity waves to emerge over a period of three years.§ An experiment was suggested by Longuet-Higgins (1962) to test the predictions made and two experiments were reported four years later which displayed many of the characteristics of the theory. The experiments were performed by Longuet-Higgins & Smith (1966) and McGoldrick, Phillips, Huang & Hodgson (1966). The interaction among deep water surface gravity waves was shown to occur at third order in the wave slope of Stokes ordering parameter $\epsilon = \kappa a$, where $\kappa = 2\pi(\text{wavelength})^{-1}$ and a is the amplitude of the same wave. As predicted, the interaction was weak and great care needed to be taken in

† Contribution no. 3209, Woods Hole Oceanographic Institution.

‡ Present address: Woods Hole Oceanographic Institution, Woods Hole, Mass. 02543.

§ See, for example, Phillips (1967) for a review of the state of the art up to 1966.

the experiments. While these experiments were being conducted, other types of waves were considered which could interact at second order in ϵ. McGoldrick (1965) suggested that capillary–gravity waves could interact at this order. Ball (1964) and Thorpe (1966) presented theoretical evidence for the interaction between surface and internal progressive gravity waves, and among internal gravity waves. Hasselmann (1966) presented a general theory for geophysical nonlinear interactions drawing an analogy with quantum field scattering theory. Experiments have recently been reported by McGoldrick (1970) and Kim & Hanratty (1971) for progressive capillary–gravity waves, and by Martin, Simmons & Wunsch (1969) for progressive internal waves. Thorpe (1966) suggested an experiment in which two progressive surface gravity waves could be made resonantly to generate an internal wave. The experiment, however, was never done. In all of the above work (except for capillary–gravity waves), at least three waves are necessary to form a set. For surface gravity waves, interactions among four waves are also possible.

It was soon realized that these theories for triad or quartet resonances could also explain the instability of a finite amplitude progressive wave. Benjamin & Feir (1967) and Phillips (1967) used these arguments to explain the ultimate breakup of a nonlinear, progressive Stokes wave due to side band resonances. Davis & Acrivos (1967) used a resonant interaction approach to explain the observed breakdown of a progressive internal wave in a diffusive, two-layer density field. Hasselmann (1967) has presented a general criterion for nonlinear wave stability. The predictions of this theory were verified by McEwan (1971) in an experiment dealing with the finite amplitude instability of standing internal waves in a linear stratification. Martin, Simmons & Wunsch (1972) reported similar instabilities for progressive internal gravity waves. Resonant nonlinear instability was suggested by Craik (1971) as an important mechanism in the turbulent breakdown of a laminar boundary layer. Clearly the importance of the resonant wave interaction mechanism has not yet been fully realized. It provides an avenue for the exchange of mechanical energy among different frequencies and scales of motion in geophysical fluids.

One possible application of this mechanism is that of the generation of oceanic internal waves by high frequency surface waves. Kenyon (1968) considered this interaction and concluded that over much of the ocean it was less important than interactions among surface or internal waves separately. For his oceanic model, he choose a constant Brunt–Väisälä frequency stratification. It will be shown in what follows that the surface–internal wave interaction can be important over much of the ocean if a near surface pycnocline is present.

An experiment has been conducted in which two high frequency surface waves are generated by a wave maker and a resonant internal wave is observed to grow. Both a constant Brunt–Väisälä and diffuse two-layer stratification are considered in detail. Unlike previous work, the experiments described here use three resonant *standing* waves in which *two* are externally produced. A theoretical approach for a rather general stratification is taken, which assumes *ab initio* all waves to be standing. The advantage of this experimental approach to the study of the interaction of surface and internal gravity waves lies

in its relative simplicity. To be more precise, the resonant growth of an internal wave can be observed as a function of time in a relatively small wave tank instead of the growth of the resonant wave with distance in a large wave tank.

In §2 the experiment will be described. Section 3 will present the theory for a general Boussinesq stratification. In §4 predictions will be compared with experimental data. A summary of the results constitutes §5.

2. Description of the experiment

2.1. *Apparatus*

The experimental work was conducted in a wave tank especially built for this study. It was constructed with plate glass sides, Plexiglas bottom and ends, and a steel frame supporting structure. The tank was 2·0 m long, 0·2 m wide and 1·0 m deep. Two Plexiglas end inserts enabled the working length of the tank to be adjusted. For most of the experiments, the length was kept at 1·8 m.

The wave tank was filled from two 55 gallon polyethylene barrels which were supported directly above the wave tank, minimizing floor space requirements. A basic state of linear density stratification was easily formed using a method suggested by Oster (1965) and used successfully by Cacchione (1970). Two reservoirs, one filled with fresh water, the other salt water, were connected via a siphon. As fresh water flowed down into the wave tank, salt water was introduced and mixed into the fresh water reservoir. An American Optical refractometer (model 10402) was used to measure the index of refraction of a millilitre sample to one part in 10^5. Calibration permitted density to be determined to five parts in 10^5. Fluid samples were withdrawn from the tank at selected depths by a one metre long hypodermic needle and syringe.

Surface waves were generated with a plunger-type paddle which was driven vertically by two synchronous motors, two eccentric drives and a mechanical adder. Eccentric driving produced higher harmonics in the vertical excursions of each shaft *before* addition. Shaft harmonics were less than 3 % of the fundamental frequency. The motion of the paddle was then a sum of the motion of the two eccentric shafts. A differential gear and a resolver were also used. The electrical output of the resolver was approximately a sinusoidal function of time with a frequency equal to the difference frequency of the two motors. Each synchronous motor had an internal gear reduction of sixteen and was driven by a stable audio oscillator and a d.c. through audio power amplifier. Continuous change of frequency of both motors was thus possible with this arrangement. One audio oscillator was a Hewlett–Packard (model 204C) with a rated stability of 0·05 %. The second frequency source was a General Radio digital frequency synthesizer (model 1161–A) with a stability of 0·01 % Net motion of the paddle was measured by a simple rack and potentiometer arrangement.

Surface-wave amplitudes were detected by a transistorized wave gauge described in detail by McGoldrick (1969). The probe itself was of the capacitance type: a replaceable piece of coated magnetic wire 0·04 in. in diameter. The amplitude and phase response of the circuitry was flat over a range of frequencies 0–10 Hz. Characteristics were not tested beyond 10 Hz. Amplitude resolution of

the whole device was limited by the ability of the experimenter to keep the fluid surface free from contaminants. A surface active agent such as Alcinox was used to reduce the surface tension at the air–'scum' interface. A sheet of saran wrap was always kept over the top of the wave tank. This helped keep the surface clean and the evaporative losses to a millimetre thick layer of water per day. With the wave gauge, resolution of 0·05 mm was possible.

The presence of internal oscillations was detected in two ways. A Sanborn differential pressure transducer (model 268 B) was used in the absolute mode to measure departures of pressure from local mean values at selected points in the fluid. The transducer proved to be a versatile and reliable instrument for both linear and diffuse two-layer stratifications alike. Fluctuations of 0·02 mm H_2O were measurable. Beardsley (1969) obtained a resolution of 5×10^{-3} mm H_2O by cross-correlating the pressure signal with a reference sinusoid of the same frequency. Depending on the density structure and frequency, a pressure resolution of 0·02 mm H_2O corresponded typically to a vertical particle excursion of 0·3 mm. Surface-wave influence was kept to a minimum by keeping the pressure probe at least one surface wavelength (20 cm) below the free surface. In addition to internal measurements, neutrally buoyant particles made to the desired density were placed in the fluid. The particles were made by mixing together carbon tetrachloride and heptane. Diphenylthiocarbazone, an intense green dye, soluble in CCL_4, increased the contrast between the particles and the background. Potassium permanganate crystals dropped into the tank during an experiment provided a visualization of the horizontal velocity field. For linear stratifications, horizontal lines of a highly non-diffusive dye (Blue Dextran 2000) were inserted during the filling process. These lines complemented the permanganate streaks by giving the field of vertical velocity. Back lighting through a diffuser enabled 16 mm moving pictures to be taken. The quantitative data for the internal oscillations, however, came from the pressure transducer and the particle amplitudes. Figure 1 shows schematically the physical location of some of the apparatus.

2.2. *Procedure*

The procedure varied with the type of experiment being done, but several steps were common to all experiments. Before stratifying the wave tank, the fluids were allowed to outgas and come to thermal equilibrium with room temperature. Ordinarily one or two days was allowed for this step. After the tank was filled, both movable ends were gently placed in position, and the surface wave paddle was inserted to its fixed equilibrium depth. The surface eigenmodes were then determined by sweeping one of the motors through a range of frequencies while observing on an oscilloscope the output of a wave gauge placed at the end opposite the wave maker. Response curves obtained were then used to select surface eigenfrequencies. A typical response curve is shown in figure 2. Prior calculation had ensured that, for the proper choices of length and depth of tank and the stratification, an internal eigenfrequency σ_{03} existed which was approximately equal to the difference frequency of a pair of surface eigenmodes σ_{01}, σ_{02}. For the generation of the fundamental internal wave (horizontal mode number of 1),

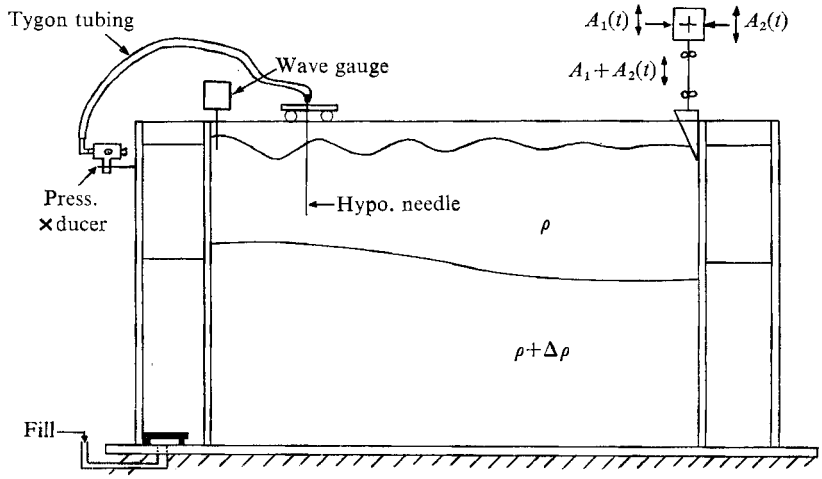

FIGURE 1. Schematic of mechanical apparatus.

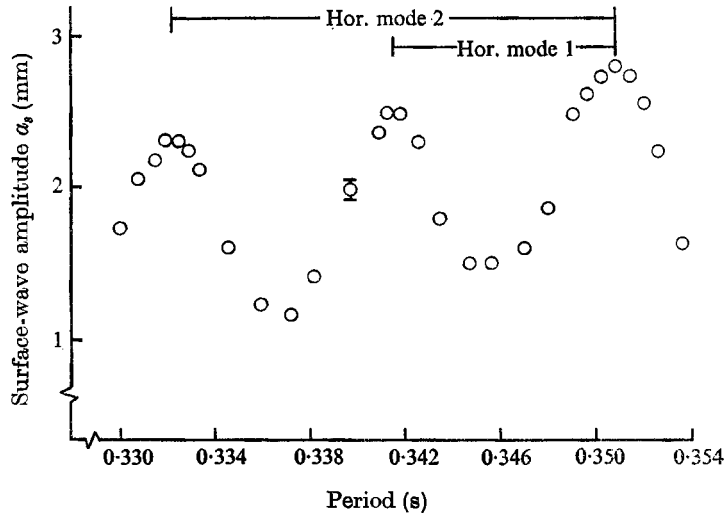

FIGURE 2. Surface-wave amplitude response against period.

two neighbouring surface-wave peaks were selected. If the second horizontal internal mode was desired, two frequencies in the surface-wave response curve were chosen so as to be separated by one peak. This is indicated in figure 2. One of the surface eigenfrequencies σ_{01} was fixed and a response curve of the internal wave was obtained by varying the second surface-wave frequency σ_2 and measuring particle and pressure amplitudes. The second surface-wave frequency σ_2 was always within 0·5 % of the eigenfrequency σ_{02}.

Initial growth to 'steady state' of the internal wave was measured with the pressure probe. One (or both) of the wave maker motors was then turned off and the viscous decay of the internal wave measured in a similar way. Since observed surface-wave decay times were an order of magnitude shorter than those of the internal waves, turning the paddle off provided after only a short lapse of time

an initial condition of no surface-wave forcing for the internal wave. In like manner, turning the paddle on provided after only a short lapse of time an initial condition of an established surface-wave field for the forcing of the resonant internal wave. The surface-wave 'response time' was typically one internal wave period.

Following each series of runs (each of which lasted a few hours), the density structure was measured and the probes were recalibrated. In the two-layer experiments, the mean position of the interface was also changed and the above procedure repeated.

While the linear stratifications remained usable for several days, the two-layer profiles needed to be 'sharpened up' every few hours. This was accomplished by siphoning off fluid from the interface region and replacing it with fresh and salty water at the top and bottom, respectively.

2.3. *Data analysis*

The analog data from the pressure and wave probes, paddle monitor, and phase resolver for each experiment were stored on tape using a Precision Instrument (model 6103) eight-track FM tape recorder. Playback in the FM mode reproduced the original signals with little distortion and permitted further analysis. During the period of resonant growth of the internal wave, data from the four sensors were played into a Sanborn four-channel strip chart recorder (model 67-1200). Playback was usually at ten times the original tape speed. This permitted the use of two Rockland active filters (model 1010F) and a PAR (Princeton Applied Research model 101) correlator. Tape loops spanning at least ten interval-wave periods were made by transcribing onto a second tape recorder. Fourier analysis of each piece permitted study of the frequency spectrum of the pressure transducer and wave gauge during the non-stationary period of growth. When a steady state was attained, the pressure and resolver signals were cross correlated and the phase was determined. The above technique agreed quite well with the 'direct' method of measurement from strip chart recorder tracings. The Fourier analysis of the surface-wave displacement was particularly interesting in the experiments in which surface eigenfrequencies were sufficiently separated so as to be adequately resolved by the correlator.

3. Theory

3.1. *Mathematical model*

The second-order or quadratic interaction among two surface gravity waves and one internal gravity wave will be considered. All waves will be assumed to be free, standing, two-dimensional waves which to lowest order in a small parameter ϵ can be described by linear, inviscid wave theory. To next higher order in ϵ (the Stokes wave slope) nonlinear and later viscous effects will be permitted. Higher-order interactions and surface tension will not be considered, the latter effect being negligible for the parameters selected.

For an incompressible, Boussinesq fluid with a zeroth-order state one of rest

and hydrostatic equilibrium the equations and boundary conditions are well known:

$$\left.\begin{aligned} \frac{D\mathbf{u}}{Dt}+\frac{1}{\rho_0}\nabla p+\mathbf{g}\frac{\rho}{\rho_0}=0, \quad & p=P_{\text{total}}-P_0, \\ \frac{D\rho}{Dt}+w\partial_z\rho_0=0, \quad & \rho=\rho_{\text{total}}-\rho_0(z), \\ \nabla.\mathbf{u}=0, & \\ \partial_z P_0=-\rho_0 g; & \end{aligned}\right\} \tag{1}$$

$$\left.\begin{aligned} P_0+p=0, \quad & z=\eta \quad \text{(free surface)}, \\ \frac{D\eta}{Dt}=w, \quad & z=\eta, \\ w=0, \quad & z=-D, \\ u=0, \quad & x=0,\, L. \end{aligned}\right\} \tag{2}$$

The boundary conditions at the free surface can be expanded in Taylor series about $z=0$. Following Thorpe (1966), the equations and boundary conditions can be put into the form

$$\{(\partial_x^2+\partial_z^2)\,\partial_t^2+N^2(z)\,\partial_x^2\}w=Q_1, \tag{3}$$

$$\{\partial_t^2\partial_z-g\partial_x^2\}w=Q_2, \quad z=0, \tag{4}$$

$$N^2\equiv-(g/\rho_0)\,\partial_z\rho_0, \tag{5}$$

$$Q_1=(g/\rho_0)\,\partial_x^2[\mathbf{u}.\nabla\rho]-\partial_x\partial_t(\partial_x[\mathbf{u}.\nabla w]-\partial_z[\mathbf{u}.\nabla u]), \tag{6}$$

$$Q_2=\partial_x\partial_t[\mathbf{u}.\nabla u]+g\partial_x^2[\eta\partial_z w-u\partial_x\eta-\partial_t(\eta\,\partial_z\phi)], \tag{7}$$

$$\phi\equiv p/g\rho_0. \tag{8}$$

Wavelike solutions of the form

$$w=a\sigma f(z)\cos\kappa x\cos(\sigma t+\theta) \tag{9}$$

have been studied for the linearized equations by many investigators (see e.g. Kraus 1966). Both a surface mode with a single maximum of velocity at the free surface and an infinite number of internal modes with maxima below the free surface are possible solutions. If the parameter $N^2/g\gamma\ll 1$, where γ is the vertical wavenumber, then the upper boundary condition for internal waves consistent with the Boussinesq approximation is that the vertical velocity must vanish.

If in addition the surface-wave frequencies are much larger than the maximum buoyancy frequency ($\sigma_{\text{surf}}^2/N_{\max}^2\gg 1$), then the deep water surface waves are not affected by the stratification. Hence linear solutions to the dynamical equations and boundary conditions are of the form

$$\left.\begin{aligned} w_j &= a_j\sigma_j f_j(z)\cos\kappa_j x\cos(\sigma_j t+\theta_j), \quad \kappa_j=n_j\pi/L, \quad n_j=1,2,\ldots, \\ u_j &= -(a_j\sigma_j/\kappa_j)f_j'(z)\sin\kappa_j x\cos(\sigma_j t+\theta_j), \quad f_j'(z)=\partial_z f(z), \\ \phi_j &= (a_j\sigma_j/g\kappa_j^2)f_j'(z)\cos\kappa_j x\sin(\sigma_j t+\theta_j), \\ \eta_j &= a_j f_j(0)\cos\kappa_j x\sin(\sigma_j t+\theta_j), \end{aligned}\right\} \tag{10}$$

where

$$f_j''+\gamma_j^2 f_j=0, \tag{11}$$

$$\gamma_j^2 = \begin{cases} -\kappa_j^2 & \text{for a surface wave,} \\ \kappa_j^2(N^2/\sigma_j^2 - 1) & \text{for an internal wave,} \end{cases} \qquad (12)$$

$$f_j(z=0) = \begin{cases} 1 & \text{for a surface wave,} \\ 0 & \text{for an internal wave.} \end{cases}$$

As is common with quadratic wave–wave interactions, the nonlinear terms may cause a slow transfer of energy and momentum among the normal modes and higher harmonics of the system. The normal modes in the limiting case of weak stratification are simply the eigenmodes of surface standing waves with no stratification and standing, rigid lid internal waves. Quadratic products in Q_1, Q_2 are of the form $\cos\kappa_n x \cos\kappa_m x$ and $\cos\kappa_n x \sin\kappa_m x$. These are expressible as sums of $\sin(\kappa_m \pm \kappa_n)x$ and $\cos(\kappa_m \pm \kappa_n)x$. It is interesting to note that if two waves in a triad of interacting waves for which $\kappa_1 \pm \kappa_2 \pm \kappa_3 = 0$ are standing, the third member, if it exists, is automatically a standing wave. Whether or not the third member of any triad exists depends upon two additional factors, the kinematic conditions that $\sigma_1 \pm \sigma_2 - \sigma_3 = 0$ *and* a non-zero interaction coefficient governing the momentum transfer among the waves of a triad. If both of these conditions are satisfied, a triad exists consisting of two surface waves and one internal wave. For any two given surface waves, the kinematic conditions can be satisfied exactly by a proper choice of N^2.

3.2. *Interaction equations*

Following earlier work (e.g. Simmons), three primary waves satisfying the dispersion relation $\sigma_{0j} = \sigma_{0j}(\kappa_j)$ to lowest order are inserted into the nonlinear equations with the amplitude and phase of each of the waves allowed to vary slowly with time. Both amplitude and phase modulation must be considered for a complete solution to the problem at this order. Six equations can be derived for the slowly varying dependent variables. If subscripts 1, 2, 3 represent the surface wave of higher frequency, lower frequency and the internal wave respectively, then for an arbitrary $N^2(z)$ the following equations can be obtained:

$$\frac{da_1}{dt} \pm \sigma_1 \frac{f_3'(0)}{4g\kappa_3}\left(1 + \frac{\sigma_3}{2\sigma_2}\right)\sigma_2\sigma_3 a_2 a_3 \cos(\theta_1 - \theta_2 - \theta_3), \qquad (13)$$

$$a_1\frac{d\theta_1}{dt} = -\sigma_1 \frac{f_3'(0)}{4g\kappa_3}\left(1 + \frac{\sigma_3}{2\sigma_2}\right)\sigma_2\sigma_3 a_2 a_3 \sin(\theta_1 - \theta_2 - \theta_3), \qquad (14)$$

$$\frac{da_2}{dt} = \sigma_2 \frac{f_3'(0)}{4g\kappa_3}\left(-1 + \frac{\sigma_3}{2\sigma_1}\right)\sigma_1\sigma_3 a_1 a_3 \cos(\theta_1 - \theta_2 - \theta_3), \qquad (15)$$

$$a_2\frac{d\theta_2}{dt} = \sigma \frac{f_3'(0)}{4h\kappa_3}\left(-1 + \frac{\sigma_3}{2\sigma_1}\right)\sigma_1\sigma_3 a_1 a_3 \sin(\theta_1 - \theta_2 - \theta_3). \qquad (16)$$

The equations for the internal wave in the triad are not obtained in so straightforward a manner as for the surface waves. The source term for the surface waves Q_2 arises from the nonlinear surface boundary condition (4). Both terms Q_1 and Q_2 must be treated for the internal wave. These forcing terms, described by Thorpe (1966) as body and surface 'forces', respectively, can be combined into

one equation and therefore compared, with the result that the body 'force' is negligible compared with the surface 'force' when surface wavelengths are much smaller than internal wavelengths.

At the free surface $z = 0$, (4) becomes for the internal mode

$$-g\partial_x^2 w_3 = Q_2, \quad z = 0, \tag{17}$$

letting

$$w_3 = \tilde{w}_3 + w_f; \tag{18}$$

then (3) becomes for $\tilde{w}_3$

$$\mathscr{L}\{\tilde{w}_3\} = -\mathscr{L}\{w_f\} + Q_1, \tag{19}$$

where

$$\mathscr{L} \equiv (\partial_x^2 + \partial_z^2)\,\partial_t^2 + N^2\partial_x^2. \tag{20}$$

The forced wave w_f and the free internal wave w_3 satisfy the boundary conditions

$$\left.\begin{aligned} \tilde{w}_3 = w_f &= 0, \quad && z = -D, \\ \tilde{w}_3 &= 0, && z = 0, \\ -g\partial_x^2 w_f &= Q_2, && z = 0. \end{aligned}\right\} \tag{21}$$

A solution w_f satisfying the boundary conditions and representing a forced second-order surface disturbance is

$$w_f = \frac{\sinh(\kappa_1 - \kappa_2)(z+D)}{g\sinh(\kappa_1-\kappa_2)D}\,\sigma_1\sigma_2\sigma_3 a_1 a_2 \cos(\kappa_1-\kappa_2)x \sin(\overline{\sigma_1-\sigma_2}t + \theta_1 - \theta_2). \tag{22}$$

An equation for the internal wave can be derived of the form

$$a_3\frac{d\theta_3}{dt}\cos(\sigma_3 t+\theta_3) + \frac{da_3}{dt}\sin(\sigma_3 t+\theta_3) = \frac{\sigma_3}{\kappa_3^2}\frac{1}{L}\frac{\int dx\cos\kappa_3 x\int dz f_3(z)[Q_1 - \mathscr{L}\{w_f\}]}{\int dz\, N^2 f_3^2(z)}. \tag{23}$$

With $f_1(z) = \exp\{k_1 z\}, f_2(z) = \exp\{k_2 z\}$

$$\mathscr{L}\{w_f\} \propto N^2\frac{\sinh(\kappa_1-\kappa_2)(z+D)}{\sinh(\kappa_1-\kappa_2)D}, \tag{24}$$

$$Q_1 \propto \sigma_3^2 \exp\{(\kappa_1+\kappa_2)z\}. \tag{25}$$

Since Q_1 decays rapidly with depth, and since $f_3(0) = 0$,

$$\int_{-D}^{0} f_3(z)\,[Q_1 - \mathscr{L}\{w_f\}]\,dz \approx -\int_{-D}^{0} f_3(z)\,\mathscr{L}\{w_f\}\,dz. \tag{26}$$

Using (26) and (23) and substituting for w_f, the equations for resonant growth of an internal wave can be written as

$$\frac{da_3}{dt} = \sigma_3 I\sigma_1\sigma_2 a_1 a_2\cos(\theta_1-\theta_2-\theta_3), \tag{27}$$

$$a_3\frac{d\theta_3}{dt} = \sigma_3 I\sigma_1\sigma_2 a_1 a_2\sin(\theta_1-\theta_2-\theta_3), \tag{28}$$

$$I = \frac{1}{2g}\frac{\int dz\, N^2 f_3(z)\sinh\kappa_3(z+D)}{\sinh\kappa_3 D\int dz\, N^2 f_3^2(z)}. \tag{29}$$

These equations, together with (13)–(16), describe the resonant energy transfer among two surface and one internal gravity wave. One interesting property of these equations, and a good check on the approximations made, is that the total energy per unit area of the three waves is constant in time.

$$E_{1,2} = \tfrac{1}{4}\overline{\rho_0} g a_{1,2}^2, \tag{30}$$

$$E_3 = \tfrac{1}{4}\overline{\rho_0} a_3^2 \int_{-D}^{0} N^2(z) f_3^2(z)\, dz, \tag{31}$$

$$\frac{dE_1}{dt} = \frac{f_3'(0)}{8g\kappa_3}\overline{\rho_0}\left(1+\frac{\sigma_3}{2\sigma_2}\right)\sigma_1\sigma_2\sigma_3 a_1 a_2 a_3 \cos(\theta_1-\theta_2-\theta_3), \tag{32}$$

$$\frac{dE_2}{dt} = \frac{f_3'(0)}{8g\kappa_3}\overline{\rho_0}\left(-1+\frac{\sigma_3}{2\sigma_1}\right)\sigma_1\sigma_2\sigma_3 a_1 a_2 a_3 \cos(\theta_1-\theta_2-\theta_3), \tag{33}$$

$$\frac{dE_3}{dt} = \frac{\overline{\rho_0}}{4}\frac{\int dz\, N^2 f_3 \sinh\kappa_3(z+D)}{\sinh\kappa_3 D}\sigma_1\sigma_2\sigma_3 a_1 a_2 a_3 \cos(\theta_1-\theta_2-\theta_3), \tag{34}$$

$$\frac{d}{dt}\left(\sum_j E_j\right) = \frac{\overline{\rho_0}}{4}\left\{\tfrac{1}{4}f_3'(0)\frac{\sigma_3}{\kappa_3}\left(\frac{1}{\sigma_1}+\frac{1}{\sigma_2}\right) + \frac{\int dz\, N^2 f_3 \sinh\kappa_3(z+D)}{g\sinh\kappa_3 D}\right\}\sigma_1\sigma_2\sigma_3 a_1 a_2 a_3 \cos(\theta_1-\theta_2-\theta_3). \tag{35}$$

It is a simple exercise to show that, consistent with the earlier assumption that $(\sigma_{1,2}/\sigma_3)^2 \gg 1$, the right-hand side of (35) vanishes.

Other integrals of the amplitude and phase equations as well as solutions to the set may be obtained following Simmons (1969), but instead simplifications will be made which will permit comparison with the experiments in which two surface waves were continuously forced by a paddle and the internal-wave amplitude was initially zero. Viscous and small detuning effects on the growing internal wave will be discussed, and a solution for the amplitude and phase of the internal wave obtained for constant surface-wave forcing. Finally, the growth rate will be evaluated for the special case of steplike and linear density fields.

3.3. *Solutions with viscosity and detuning for constant surface waves*

Following McGoldrick (1965, 1970), McEwan (1971) and Kim & Hanratty (1971), each mode will be assumed to decay independently. An unforced mode j will decay at a rate $\dot{a}_j/a_j = -\lambda_j$, where $(\dot{}) \equiv d/dt$. The decay factor λ_j is independent of amplitude a_j and depends upon viscosity, wavelength, frequency and the geometry of the tank. The primary source of internal-wave viscous dissipation for the parameters used in the laboratory experiment was due to side wall boundary layers. For the steplike, two-layer model an additional interior shear layer at the interface was also important. The decay factor can be found experimentally and theoretically. It is presented in the appendix for the interfacial wave and has been derived by McEwan (1971) for a linear stratification. For the present, λ_j will be assumed known. To be consistent with earlier approximations, the fluid must be only slightly viscous ($\lambda_j/\sigma_j \ll 1$). Since solutions for surface-wave ampli-

tudes are not obtained, only internal-wave damping will be included in what follows. Focussing on the internal-wave amplitude and phase equations, λ_j will appear only in the amplitude equation for $\dot{a}_3$.

An additional parameter δ will be introduced to represent the deviation of the forcing frequency $\sigma_3 = \sigma_1 - \sigma_2$ from the natural response frequency of an internal wave σ_{03} having a horizontal wavenumber $\kappa_3 = \kappa_1 - \kappa_2$. Thus

$$\sigma_3 = \sigma_{03}(1+\delta), \quad |\delta| \ll 1. \tag{36}$$

Following Joyce (1972), (27), (28) for the internal wave become

$$\frac{da_3}{dt} + \lambda_3 a_3 = \sigma_3 I a_1 a_2 \sigma_1 \sigma_2 \cos(\theta_1 - \theta_2 - \theta_3), \tag{37}$$

$$a\frac{d\theta_3}{dt} + \delta\sigma_3 a_3 = \sigma_3 I a_1 a_2 \sigma_1 \sigma_2 \sin(\theta_1 - \theta_2 - \theta_3). \tag{38}$$

For $a_1, a_2, \theta_1, \theta_2$ constant, solutions for a_3, θ_3 may be obtained subject to the initial condition of zero amplitude for a_3. Several special solutions will also be presented.

(i)
$$\left.\begin{aligned} &\delta = 0, \quad \lambda_3 = 0, \\ &\theta \equiv \theta_3 - \theta_1 + \theta_2 = \begin{cases} 0 & (\operatorname{sgn} I > 0), \\ \pi & (\operatorname{sgn} I < 0), \end{cases} \\ &a_3 = |\hat{I}|t, \quad \hat{I} \equiv I a_1 a_2 \sigma_1 \sigma_2 \sigma_3. \end{aligned}\right\} \tag{39}$$

(ii)
$$\left.\begin{aligned} &\delta = 0, \quad \lambda_3 \neq 0, \\ &\theta = \begin{cases} 0 & (\operatorname{sgn}\hat{I} > 0), \\ \pi & (\operatorname{sgn}\hat{I} < 0), \end{cases} \\ &a_3 = (|\hat{I}|/\lambda_3)(1 - \exp\{-\lambda_3 t\}). \end{aligned}\right\} \tag{40}$$

(iii)
$$\left.\begin{aligned} &\delta \neq 0, \quad \lambda_3 = 0, \\ &\theta = \begin{cases} -\frac{1}{2}\delta\sigma_3 t & (\operatorname{sgn}\hat{I} > 0), \\ \pi - \frac{1}{2}\delta\sigma_3 t & (\operatorname{sgn}\hat{I} < 0), \end{cases} \\ &a_3 = |\hat{I}|\, t \frac{\sin(\frac{1}{2}\delta\sigma_3)t}{(\frac{1}{2}\delta\sigma_3)t}. \end{aligned}\right\} \tag{41}$$

(iv)
$$\left.\begin{aligned} &d/dt = 0, \\ &\theta = \theta^0 = \operatorname{sgn}\hat{I} \tan^{-1}(\delta\sigma_3/\lambda_3), \\ &a_3 = a_3^0 = \frac{|\hat{I}|}{[\lambda_3^2 + (\delta\sigma_3)^2]^{\frac{1}{2}}}. \end{aligned}\right\} \tag{42}$$

(v) The full solution, retaining all terms, is

$$\left.\begin{aligned} \tan\theta &= \tan\theta^0 \left[\frac{1 - \exp\{-\lambda_3 t\}\cos\delta\sigma_3 t - (\lambda/\delta\sigma)\exp\{-\lambda_3 t\}\sin\delta\sigma_3 t}{1 - \exp\{-\lambda_3 t\}\cos\delta\sigma_3 t + (\delta\sigma_3/\lambda_3)\exp\{-\lambda_3 t\}\sin\delta\sigma_3 t}\right]^{\frac{1}{2}}, \\ a_3 &= a_3^0[1 + \exp\{-2\lambda_3 t\} - 2\exp\{-\lambda_3 t\}\cos\delta\sigma_3 t]^{\frac{1}{2}}. \end{aligned}\right\} \tag{43}$$

The solutions obtained above are valid only when surface-wave amplitudes remain constant. As an internal wave of amplitude equal to a surface wave has

	σ_{01} (rad s^{-1}) σ_{02}	σ_{03} σ_{03} (linear theory)	a_1 (mm)	a_2 (mm)	a_3 (mm)	n	ρ_{max}	N_{max} (rad s^{-1})
E1c	18·20 17·72	0·484 0·492	3·77	2·68	5·5	1	1·049	4·9
E2	18·91 17·88	1·034 1·015	2·79	2·36	5·75	2	1·077	4·76
E3	18·20 17.71	0·493 0·488	3·75	2·68	4·75	1	1·116	$\bar{N}$ 1·10

TABLE 1

only a fraction of the energy, it was thought for the experiments that these solutions would approximately hold throughout the resonant growth to a steady state determined by the surface forcing and viscosity. Comparison with the data will show the above assumption to be valid for small internal waves (away from the peak response), but invalid when internal-wave amplitudes become large.

3.4. *Evaluation of interaction term for two special cases*

The theoretical approach thus far has been valid for a Boussinesq fluid with arbitrary stratification. Two simple cases (both analytically and experimentally) are a two-layer and a linear stratification. Accordingly, then, the interaction terms I for the two cases are

$$N^2 = g\frac{\Delta\rho}{\rho_0}\delta_d(z+d), \quad I = -\frac{\sinh\kappa_3(D-d)}{2g\sinh\kappa_3 D\sinh\kappa_3 d}, \tag{44}$$

$$N^2 = \text{const.}, \quad I = \frac{(-1)^{m+1}}{gm\pi}[1+(\kappa_3 D/m\pi)^2]^{-1}, \tag{45}$$

where m is the vertical mode number (1, 2, 3, ...).

4. Results

Data from these basic experiments will be presented and compared with theory for the special cases of a steplike density profile (experiments 1 and 2) and a linear profile (experiment 3). As many of the results will be similar for all three cases, only experiment 1 will be discussed in detail. In experiments 1 and 3 the fundamental ($n = 1$) horizontal internal mode was generated, while experiment 2 studied the growth of the $n = 2$ mode. Table 1 shows a summary of experimental parameters, and figure 3 presents profiles of $N^2(z)$ for all three experiments. Deviation of N^2 from theoretical ideals caused theoretical and experimental eigenfrequencies to differ by as much as 2%. Anticipated frequencies were adjusted to take this into account.

In experiment 1 (E1), the fundamental 'interfacial' wave was selected as the third member of the triad. Its observed steady-state amplitude response obtained from the pressure transducer and particle motion is shown for each of three

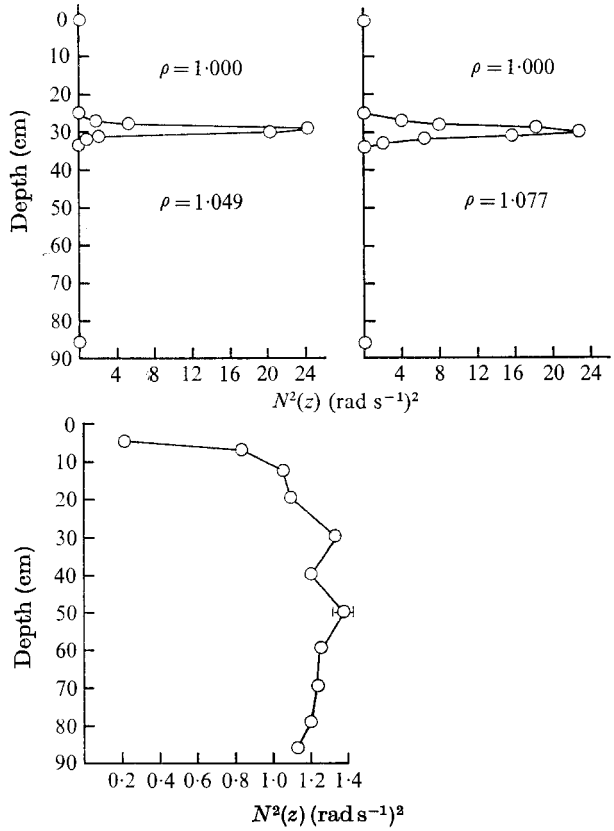

FIGURE 3. Profiles of N^2 against depth for E1*c* (upper left), E2 (upper right) and E3.

interface depths in figure 4. The intensification of the response as the interface was raised from 50 cm (●) to 40 cm (○), two surface wavelengths from the free surface, is apparent. The predicted response for an interface depth of 30 cm shows good agreement away from the peak, but overshoots the observed amplitude for small δ. The steady-state phase response for the same example (henceforth E1*c*) in figure 5 was obtained by cross-correlating the pressure signal with the resolver reference signal. Except for the case of $\delta = 0$, all phases were underpredicted. This could partly be a result of the correlation technique, which averaged over phases that were, in many cases, still increasing away from π.

All theoretical curves for steady-state response depend strongly upon the internal-wave dissipation parameter $\lambda = \lambda_3$. This quantity was measured independently from the resonant interaction by turning *both* surface wave motors off, and observing the decay of a tuned internal wave. Later the effect of turning off only one, rather than two, of the motors will be shown. In figure 6, the decay of the free mode ($T = 12{\cdot}98$ s) is shown along with a theoretical rate obtained (in the appendix) assuming side wall boundary layers and an internal shear layer at an interface of constant N^2 with thickness l. The parameter $\lambda \sim O(Re)^{-\frac{1}{2}}$,

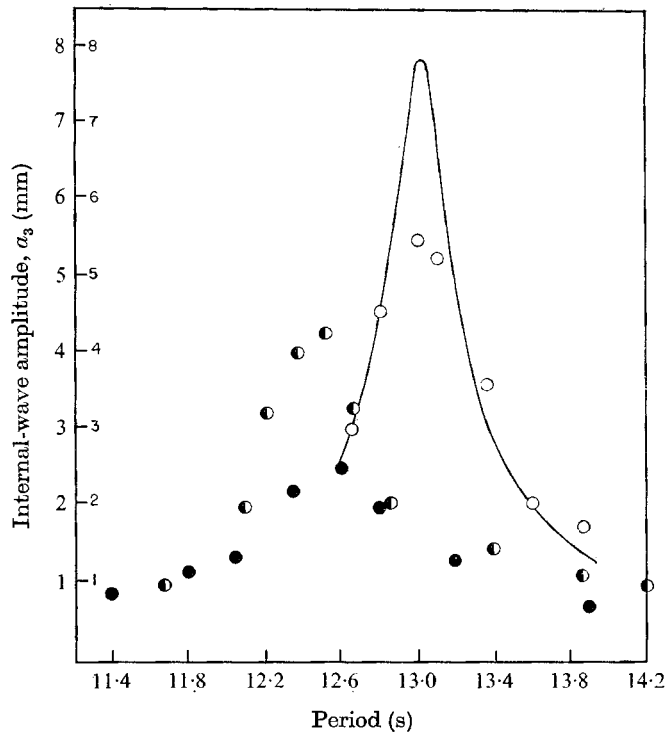

FIGURE 4. Internal-wave amplitude response against period for interface depth of 50 (●), 40 (◐) and 30 cm (○). Data here and in subsequent figures show pressure measurements converted to amplitude of internal-wave vertical displacement. Frequency shift above is due to change of mean interface depth to 15 cm above mid-depth.

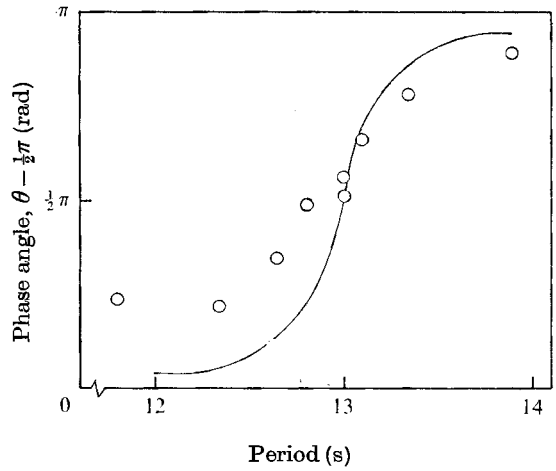

FIGURE 5. Phase response against period for E1*c*.

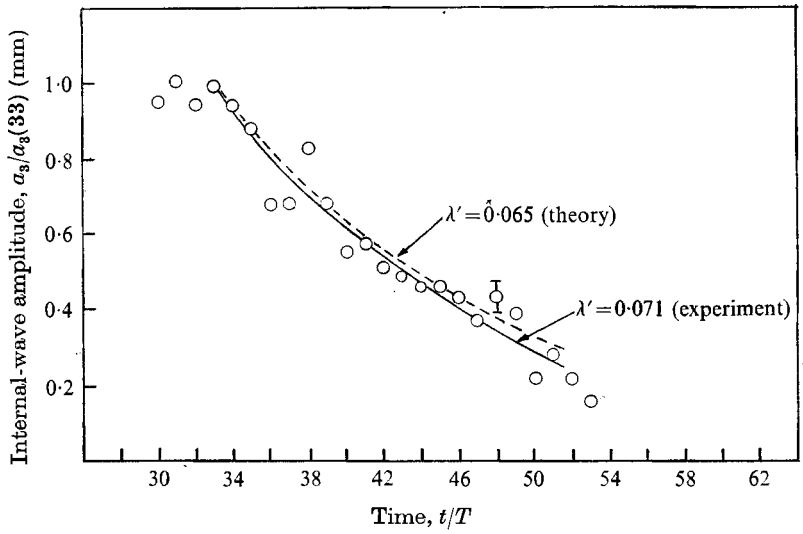

FIGURE 6. Viscous decay of free mode interfacial wave in E1c with $\lambda' = (2\pi/\sigma_3)\lambda_3$. Paddle forcing stopped at $t/T = 32$. Axes are $a_3(t/T)/a_3(33)$ against t/T, $T = 12{\cdot}98$ s.

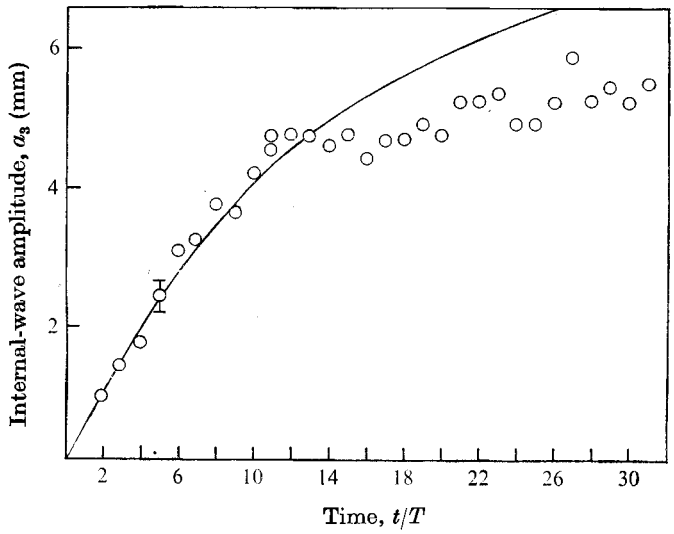

FIGURE 7. Resonant growth of a tuned internal wave in E1c; $a_3(t/T)$ against t/T, $T = 12{\cdot}98$ s.

where $Re^{-1} = \nu\kappa^2/\sigma$ and ν is the dynamic viscosity. In all cases where some discrepancy in expected and measured decay rates existed, measured rates were used.

The resonant growth from zero amplitude a_3 of the tuned internal wave is shown in figure 7. When the amplitude reached 90 % of its final value (5·5 mm), the observed growth rate suddenly decreased from the predicted, viscously limited curve. For large t/T one continues to see an increasing discrepancy which

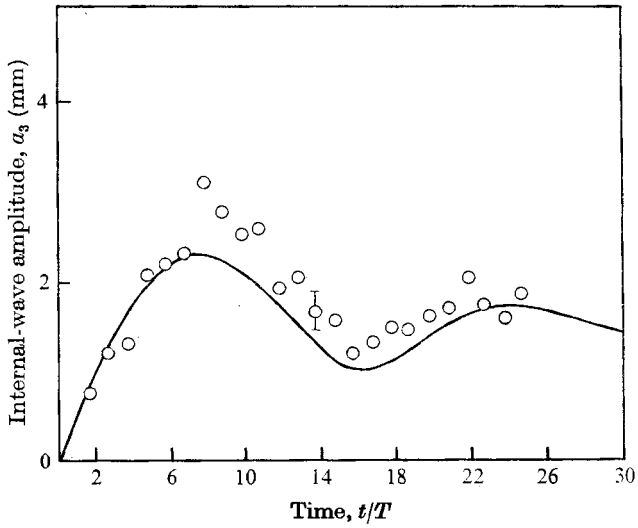

FIGURE 8. Resonant growth of a detuned ($\delta = -0{\cdot}061$) internal wave in E1*c*; a_3 (t/T) against t/T; $t = 13{\cdot}85$ s.

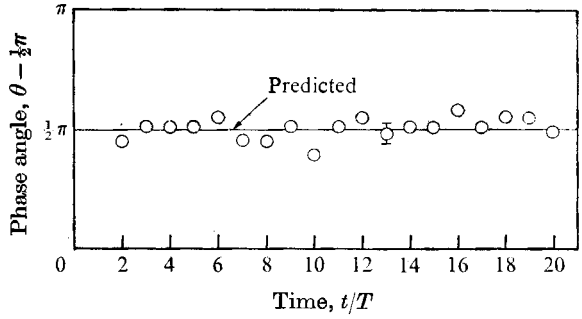

FIGURE 9. Phase, $\theta - \frac{1}{2}\pi$, of a tuned internal wave in E1*c* against t/T, $T = 12.98$ s.

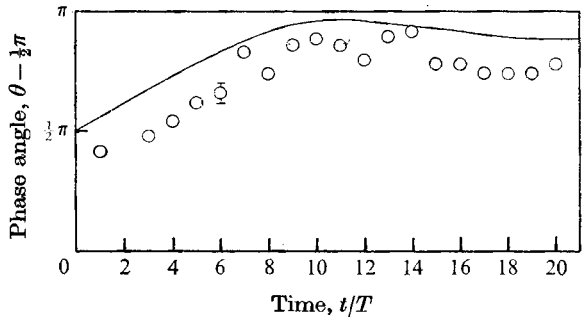

FIGURE 10. Phase, $\theta - \frac{1}{2}\pi$, of a detuned ($\delta = -0{\cdot}061$) internal wave in E1*c* against t/T, $T = 13{\cdot}85$ s.

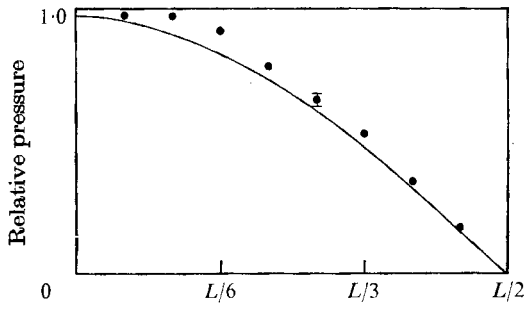

FIGURE 11. Dependence of pressure upon horizontal position for the tuned $n = 1$ internal wave of E1*c*, $z = -13$ cm, $L = 2D = 180$ cm.

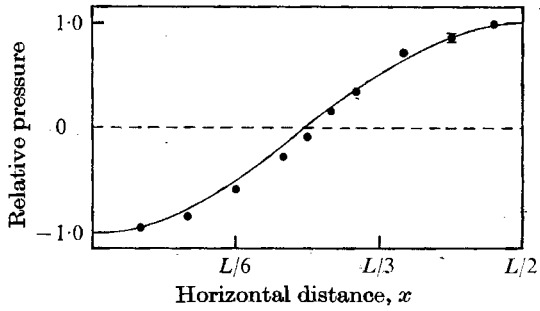

FIGURE 12. Dependence of pressure upon horizontal position for the tuned $n = 2$ internal wave of E2, $z = -13$ cm, $L = 2D = 180$ cm.

was evident in the steady-state response (figure 4). The resonant growth of a detuned wave is presented in figure 8. A small constant offset between theory and experiment is apparent in this figure. The temporal variation of phase $\theta \equiv \theta_3 - \theta_1 + \theta_2$ for the tuned and detuned cases is shown in figures 9 and 10, respectively. As expected, one sees that for $\delta = 0$ the initial phase demanded by the interaction remains constant for the duration of the experiment. With $\delta \neq 0$, in figure 10 the phase drifts, initially linearly, finally reaching a value fixed by the detuning and viscosity. For the detuned case, the measured and predicted phase and amplitude (figure 8) differ by a constant offset. These two discrepancies are coupled, and could conceivably both be accounted for by a single unknown cause.

Many of the above results were repeated in later experiments. Experiment 2 was designed to generate a second interfacial mode in the horizontal, rather than $n = 1$. To show that both of these modes were actually involved in each experiment figures 11 and 12 indicate changes in measured pressure with horizontal position at a fixed depth for E1*c*, E2, respectively, with cosine dependence of the expected perturbation pressure field included.

If one were to present the clearest agreement with theory for any of the various cases (tuned or detuned growth, steady-state response curves), one would choose E2 as a 'typtical' example. To show this, figure 13 indicates

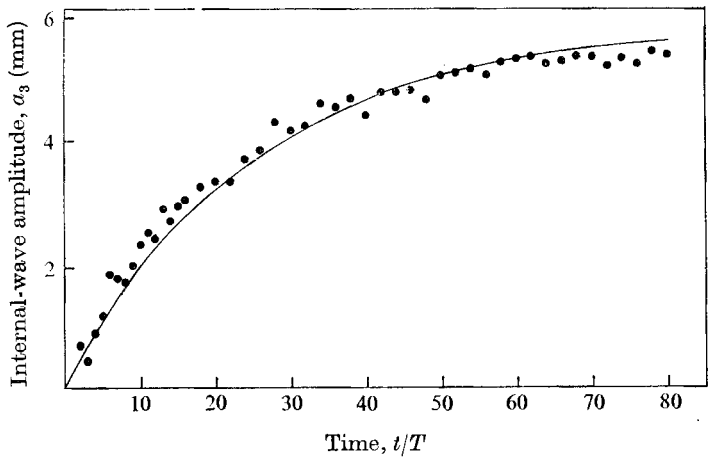

FIGURE 13. Resonant growth of a tuned second horizontal mode ($n = 2$) internal wave in E2; $a_3\,(t/T)$ against t/T, $T = 6{\cdot}08$ s.

the growth to steady state of the internal wave in E2. Because of the shorter period of this wave (as opposed to E1), more observations were possible, and a greater separation in surface-wave frequencies permitted a detailed spectral study of the surface-wave displacement throughout E2. In all three experiments, slight distortions in the modulated surface displacement appears (for the cases of large internal-wave response) after several internal-wave periods. These distortions in the regular modulation were resolved in E2 and will be presented at the end of this section. Their nature indicates that such good agreement as shown in figure 13 was rather fortuitous!

In E3 an $n = 1$, $m = 1$ internal wave was generated, where m is the vertical mode number of this constant N^2 experiment. The growth to steady state of both a tuned and a detuned wave in figure 14 bears much resemblance to E1 with the exception that observations tended to be more erratic. It is suspected that, for the continuously-stratified case, transient and other noise no longer confined to the interface (e.g. higher modes) interfered with the detection of the resonant mode. That the resulting wave was the $m = 1$ mode is verified by figure 15, which shows the variation of the steady-state pressure with x (top) and z (bottom). In E3 the viscous decay of the free $n = m = 1$ mode was examined when one and both motors were turned off. The latter case simulated pure viscous decay of an unforced mode, while in the former case an additional high frequency surface wave was present. Figure 16 indicates that decay was faster with one motor off than with both off. Least squares regression lines for both λ's have been drawn (open circles) on figure 16. The explanation for the difference is simple; with a single, forced surface wave present, the decaying internal wave could resonantly excite a second surface wave thereby losing energy faster. An examination of the surface displacement clearly showed that this was true: a modulation of the displacement indicative of the presence of a second surface wave continued long after (200 surface wave periods) the forcing paddle had been disengaged.

In E2 surface-wave amplitude spectra were computed using the PAR

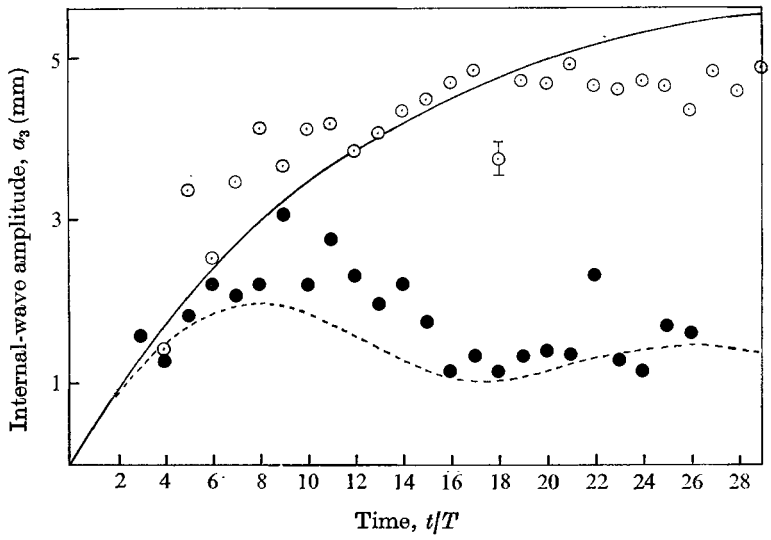

FIGURE 14. Resonant growth of a tuned (⊙) and detuned (●, $\delta = 0{\cdot}056$) fundamental internal mode ($n = m = 1$) in E3, $T_{res} = 12{\cdot}75$ s.

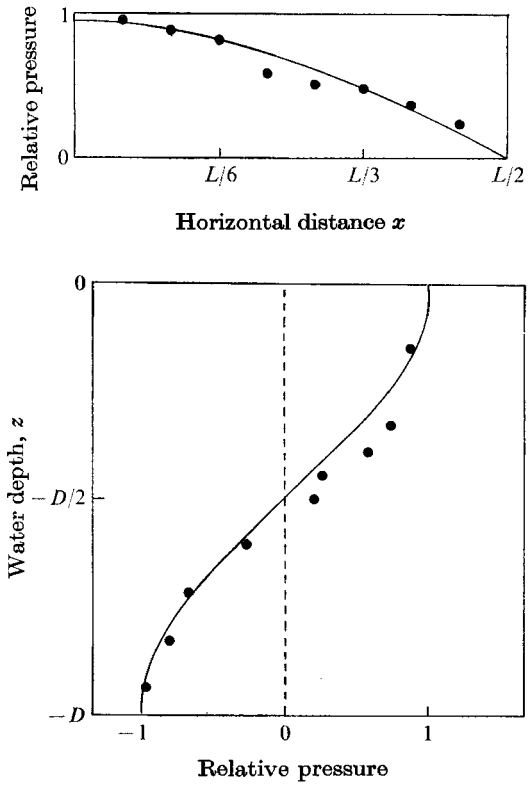

FIGURE 15. Pressure dependence upon horizontal position (upper) with $z = -13$ cm and with depth (lower) for $x = 20$ cm in E3. $L = 2D = 180$ cm.

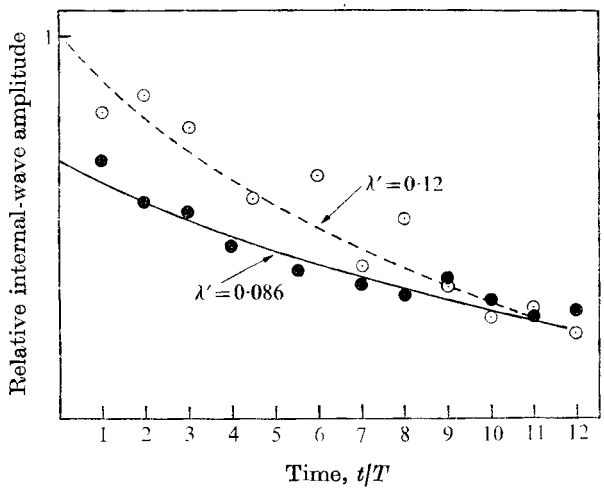

FIGURE 16. Observed effect of the nonlinear interaction upon the time decay of the fundamental internal mode in E3. Decay over-plotted of two different experimental conditions (see text), showing relative internal-wave amplitude against t/T, $\lambda' = (2\pi/\sigma_3)\lambda_3$, $T = 12{\cdot}75$ s.

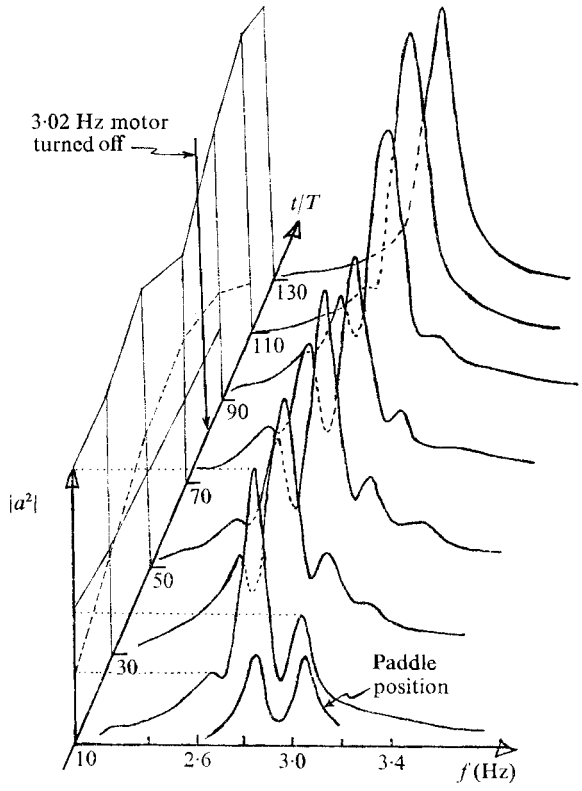

FIGURE 17. Development of surface-wave displacement spectrum at $x = 0$ with non-dimensionalized time t/T during resonant growth of $n = 2$ tuned internal wave of E2. Successive spectra represent averages over 20 record lengths, each length containing 20 surface-wave periods, $T = 6{\cdot}08$ s.

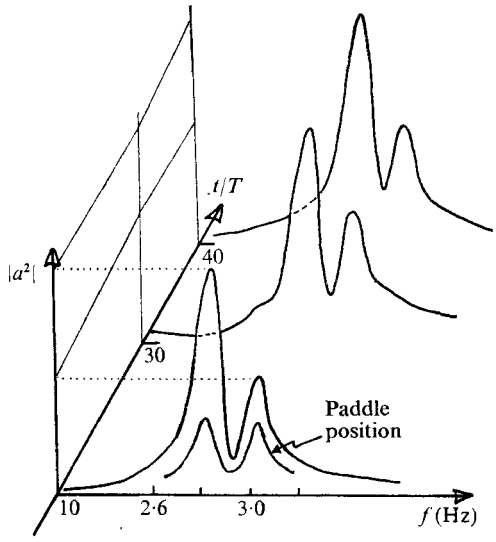

FIGURE 18. As figure 17, but with detuned ($\delta = -0{\cdot}033$) internal wave in E2, $T = 6{\cdot}28$ s.

correlator and Fourier analyser with tape loops containing approximately 400 surface waves with 20 modulations. A record length for computation of 35 surface-wave periods was chosen, long enough to resolve two frequencies differing by 6 % (16 surface-wave periods), yet short enough to prevent instrumental aliasing in the correlator (50 surface-wave periods). Spectra shown in figures 17 and 18 represent averages over each tape loop (20 internal-wave periods). The change in the spectrum with time is indicated by successive surface-wave spectra from different tape loops. The paddle spectrum is included for reference.

The spectra for the *tuned* internal wave of figure 13 are shown in figure 17. The general trend indicates a steady loss of energy by the paddle-forced wave of higher frequency and a growth of a third surface wave of lower frequency which, being unforced by the paddle, was initially absent. Other lumps at higher and lower frequencies appear, but these remain small. The new surface wave at 2·65 Hz, however, eventually becomes as large as the initial paddle-forced wave. The rate of change of the spectrum becomes less after 50 internal-wave periods. It is not clear that any asymptotic state had been reached before one of the motors was turned off ($t/T = 80$), causing a decay of the internal wave and all but one of the surface waves. Figures 14 and 18 together provide a complete picture of the important waves involved in this experiment. What is amazing is the good agreement with a theory which assumes no change in the surface-wave spectrum. It will be explained shortly that most of the details of the surface-wave field are lost upon the internal wave, whose growth depends upon products of surface-wave amplitudes and their relative phases.

In E2 a detuned internal wave of period 6.28 s was generated having a final amplitude of 25 % of that for the tuned wave just discussed. Its final amplitude was predicted to within the experimental error. The surface-wave spectrum of

figure 18 indicates no significant change throughout the growth to steady state of the detuned, resonant internal wave.

During one of the experiments it was observed on one occasion that a single surface wave of large amplitude became unstable to another surface wave of lower frequency and an internal wave. This effect of a critical amplitude on stability of a single wave, though not studied in detail, is similar to observations made by Davis & Acrivos (1967), McEwan (1971) and Martin, Simmons & Wunsch (1972).

The development of the surface-wave field can be understood by reference to the energy transfer equations (32)–(34) for the triad resonance. While the energies of each of the two surface waves can change significantly owing to the presence of an internal wave, the actual transfer from the surface-wave field to the internal wave remains small owing to cancellation of large terms when the sum of the changes for both surface waves is found. For resonant growth of the internal wave a_3, the interaction requires that $\mathrm{sgn}[f_3'(0)\cos(\theta_1-\theta_2-\theta_3)] = -1$ in (32), (33). Hence the surface wave of higher frequency loses energy, most of which goes to the other surface wave. The growing waves can in turn form a triad with a new surface wave having a lower frequency than either of the other two and which is not directly forced by the paddle.

The internal-wave growth rate is practically unaffected by energy exchanges between the two surface waves in a triad, because of its low demand upon net surface-wave energy, and because the product $a_1 a_2$ of surface-wave amplitudes appearing in the transfer term in (27) remains nearly constant. Additional surface waves generated continue to contribute to sustained internal-wave growth if their relative phases are correct. The details of the development of the surface-wave spectrum, including nonlinearity, paddle forcing and dissipation, are beyond the scope of this work. We wish only to indicate that observations in contradiction with the restrictive assumption of constant surface-wave forcing are not inconsistent with (13)–(16), (27)–(29).

5. Summary

Theoretical results for the nonlinear interaction among two standing surface waves and one standing internal wave were specialized for two-layer and linear stratifications. Comparison with experiments showed that the paddle-forced surface waves remained constant and the resonantly excited internal-wave growth was predicted quite well for small internal-wave amplitudes, when both viscous effects and slight detuning were included in the model. When internal-wave amplitudes became large, however, the surface-wave field became distorted, with at least one additional surface wave of lower frequency than the original two, gaining energy at the expense of the surface wave of highest frequency. The resulting internal wave was of lower amplitude than would be anticipated for a constant surface-wave field. The new surface wave in all cases formed a resonant triad with the internal wave and intermediate frequency surface wave.

In agreement with Hasselmann's (1967) stability criterion, the wave of highest frequency in the triad initially loses energy to the other two. A preferential

direction exists then for energy transfer to lower frequencies in the surface-wave field. The internal wave in a triad exchanges only a fraction of the total energy with the surface waves, yet a large exchange of energy takes place within the surface-wave field owing to the presence of the internal wave. The latter, if of sufficiently large amplitude, acts as a catalyst, promoting energy transfer among surface waves to a lower order, formally, than deep water surface-wave self-interactions.

The strength of the interaction is dependent from (29) upon the overlapping of the surface forcing and the vertical eigenfunctions of the internal modes. Hence the presence of a seasonal, or shallow, pycnocline would enhance the interaction term (the term decreases exponentially as an interface is removed from the free surface). If one compares the ratio of the interaction coefficients derived for the two-layer and linear stratifications, one finds that, in the limit as $\kappa_3 D \gg 1$, $\kappa_3 d \sim O(1)$ (infinitely deep ocean, shallow pycnocline),

$$\frac{I_{n=\text{const.}}}{I_{2-\text{layer}}} \sim \frac{\exp\{\kappa_3 d\}}{2(\kappa_3 D)^2} \ll 1,$$

where $D(d)$ is the total (interface) depth, and κ_3 is the vertical wavenumber of the surface forcing. Results of this paragraph hold for progressive as well as standing waves. Thus, an internal wave trapped on a shallow density interface would be much more receptive to second-order nonlinear resonant interactions with surface gravity waves for an oceanic system.

The author is indebted to the staff in the Department of Meteorology at M.I.T., especially Prof. Robert Beardsley, for their help and guidance. The work was sponsored at M.I.T. by an N.D.E.A. Title IV fellowship, National Science Foundation grant GP-5053 and Office of Naval Research contract N00014-67-A-0204-008 and completed at W.H.O.I. under sponsorship of the Johns Hopkins University Applied Physics Laboratory under contract 372111.08.

Appendix. Evaluation of viscous dissipation for a diffuse two-layer system

A two-layer model of total density difference $\Delta\rho$ will be considered, in which the interfacial region is characterized by a thin transition layer of thickness l centred at a depth d, with a constant N such that $(N/\sigma)^2 \gg 1$. The dissipation of total mechanical energy E of a two-dimensional internal wave of frequency σ, wavenumber κ, in a tank of width W, length L, and depth D can be written as

$$\dot{E} = -2\lambda E, \tag{A 1}$$

where $\lambda = \lambda^{(1)} + \lambda^{(2)}$ arises chiefly from dissipation at the interface and rigid wall boundary layers, respectively.

(i) Interface region. In this region

$$\{\partial_t^2(\partial_x^2 + \partial_z^2) + N^2\partial_x^2\} w \sim \{\partial_t^2 \partial_z^2 + N^2\partial_x^2\} w = 0. \tag{A 2}$$

Phillips (1966) considered an inviscid model similar to this and obtained simple solutions for the velocities. Within the layer, the dissipation per unit horizontal area is

$$\int_{-d-\frac{1}{2}l}^{-d+\frac{1}{2}l} dz\mu \left(\frac{\partial u}{\partial z}\right)^2 \sim \mu \left(\frac{\partial u}{\partial z}\right)^2 l. \tag{A 3}$$

Substituting for the velocities and solving for $\lambda^{(1)}$, one can obtain

$$\lambda^{(1)} = (Re^{-1}) N^2/\sigma^2, \tag{A 4}$$

$$Re^{-1} \equiv \nu\kappa^2/\sigma \ll 1. \tag{A 5}$$

(ii) If $\mathbf{q}_i \cos(\sigma t + \theta)$ is the interior velocity of the standing internal wave ($\mathbf{q}_i = \mathbf{q}_i(x, z)$), then the total velocity field satisfying a no-slip boundary condition at a rigid wall is

$$\left.\begin{aligned} \mathbf{q}_T &= \mathbf{q}_i[\cos(\sigma t + \theta) - \exp(-\zeta)\cos(\sigma t + \theta - \zeta)], \\ \zeta &= \gamma(\sigma/2\nu)^{\frac{1}{2}}. \end{aligned}\right\} \tag{A 6}$$

γ is a co-ordinate normal to the rigid surface. The total dissipation per unit area in the boundary layer is

$$\mu \int_0^\infty d\zeta \left(\frac{2\nu}{\sigma}\right)^{\frac{1}{2}} \left[\frac{d\mathbf{q}_T}{\partial\gamma} \cdot \frac{\partial \mathbf{q}_T}{\partial\gamma}\right]. \tag{A 7}$$

Since little horizontal oscillatory motion was observed at the free surface, it will be considered a no-slip surface. For a standing internal-wave field, and a thin boundary layer (satisfied if $Re^{-1} \ll 1$), one can derive

$$\lambda^{(2)} = \tfrac{1}{2}\sigma Re^{-\frac{1}{2}} Q,$$

$$Q = \frac{2}{\kappa W} + \frac{2}{\kappa L} + \frac{\rho[1 + 2d/L]\sinh^{-2}\kappa d + (\rho + \Delta\rho)[1 + (D-d)/L]\sinh^{-2}\kappa(D-d)}{\rho\coth\kappa d + (\rho + \Delta\rho)\coth\kappa(D-d)}. \tag{A 8}$$

Combining the results of (i) and (ii), one obtains

$$\lambda = \tfrac{1}{2}\sigma\, Re^{-\frac{1}{2}}[Q + 2(N^2/\sigma^2)\, Re^{-\frac{1}{2}}] + O(Re^{-1}, l/D\, Re^{-\frac{1}{2}})\,\sigma. \tag{A 9}$$

REFERENCES

Ball, F. K. 1964 Energy transfer between external and internal gravity waves. *J. Fluid Mech.* **19**, 465.

Beardsley, R. C. 1969 An experimental study of inertial waves in a closed cone. *M.I.T. Geophysical Fluid Dynamics Laboratory Rep.* GFD/69-1.

Benjamin, T. B. & Feir, J. E. 1967 The disintegration of wave trains on deep water. *J. Fluid Mech.* **27**, 417.

Cacchione, D. A. 1970 Experimental study of internal gravity waves over a slope. Ph.D. thesis, M.I.T.–W.H.O.I. Joint Program in Oceanography.

Craik, A. D. D. 1971 Nonlinear resonant instability in boundary layers. *J. Fluid Mech.* **50**, 393.

Davis, R. E. & Acrivos, A. 1967 The stability of oscillatory internal waves. *J. Fluid Mech.* **30**, 723.

Hasselmann, K. A. 1966 Feynman diagrams and interaction rules of wave–wave scattering processes. *Rev. Geophys.* **4**, 1.

Hasselmann, K. A. 1967 A criterion for nonlinear wave stability. *J. Fluid Mech.* **30**, 737.

JOYCE, T. M. 1972 Nonlinear interactions among standing surface and internal gravity waves. Sc.D. thesis, M.I.T.–W.H.O.I. Joint Program.

KENYON, K. 1968 Wave–wave interactions of surface and internal waves. *J. Mar. Res.* **26**, 208.

KIM, T. K. & HANRATTY, T. J. 1971 Weak quadratic interactions of two-dimensional waves. *J. Fluid Mech.* **50**, 107.

KRAUS, W. 1966 *Interne Wellen.* Berlin-Nikolassee: Gebrüder Borntraeger.

LONGUET-HIGGINS, M. S. 1962 Resonant interactions between two trains of gravity waves. *J. Fluid Mech.* **12**, 321.

LONGUET-HIGGINS, M. S. & SMITH, N. D. 1966 An experiment on third-order resonant wave interactions. *J. Fluid Mech.* **25**, 417.

MCEWAN, A. D. 1971 Degeneration of resonantly-excited standing internal gravity waves. *J. Fluid Mech.* **50**, 431.

MCGOLDRICK, L. F. 1965 Resonant interactions among capillary gravity waves. *J. Fluid Mech.* **21**, 305.

MCGOLDRICK, L. F. 1969 A system for the generation and measurement of capillary-gravity waves. *Department of the Geophysical Sciences, University of Chicago, Tech. Rep.* no. 3.

MCGOLDRICK, L. F. 1970 An experiment on second-order capillary–gravity resonant wave interactions. *J. Fluid Mech.* **40**, 251.

MCGOLDRICK, L. F., PHILLIPS, O. M., HUANG, N. & HODGSON, T. 1966 Measurements on resonant wave interactions. *J. Fluid Mech.* **25**, 437.

MARTIN, S., SIMMONS, W. F. & WUNSCH, C. 1969 Resonant internal wave interactions. *Nature*, **224**, 1014.

MARTIN, S., SIMMONS, W. F. & WUNSCH, C. 1972 The excitation of resonant triads by single internal waves. *J. Fluid Mech.* **53**, 17.

OSTER, G. 1965 Density gradients. *Scientific American*, **213**, 70.

PHILLIPS, O. M. 1960 On the dynamics of unsteady gravity waves of finite amplitude. *J. Fluid Mech.* **9**, 193.

PHILLIPS, O. M. 1966 *Dynamics of the Upper Ocean.* Cambridge University Press.

PHILLIPS, O. M. 1967 Theoretical and experimental studies of gravity wave interactions. *Proc. Roy. Soc.* A **299**, 104.

SIMMONS, W. F. 1969 A variational method for weak resonant wave interactions. *Proc. Roy. Soc.* A **309**, 551.

THORPE, S. A. 1966 On wave interactions in a stratified fluid. *J. Fluid Mech.* **24**, 737.